OPEN ACCESS
IOP Publishing
Classical and Quantum Gravity
Class. Quantum Grav. **42** (2025) 235007 (21pp) https://doi.org/10.1088/1361-6382/ae2058

Telescopes for LISA: function, current status, and path forward

Mateo Batkis[1], Joshua Berrier[1], Kevin Boyce[1], John Capone[1], Ryan Derosa[1], Joseph Howard[1], Joseph Ivanov[2], Craig Jones[3], Jason Kelly[3], Ritva Keski-Kuha[1], Joshua Lutter[3], Andrew Menas[4], Nicolas Nicolaeff[4], Nova Nimmo[5], Jonathan Papa[1], Shannon Sankar[6,7,*], Shane Wake[1] and Andrew Weaver[4]

[1] National Aeronautics and Space Administration, Greenbelt, Maryland, United States of America
[2] Newton, LLC, Greenbelt, Maryland, United States of America
[3] KBR Inc., Greenbelt, Maryland, United States of America
[4] Aerodyne Industries, Greenbelt, Maryland, United States of America
[5] Peraton Inc., Greenbelt, Maryland, United States of America
[6] University of Maryland at College Park, College Park, Maryland, United States of America
[7] Center for Research and Exploration in Space Science and Technology, Greenbelt, Maryland, United States of America

E-mail: shannon.r.sankar@nasa.gov

Received 30 June 2025; revised 22 September 2025
Accepted for publication 17 November 2025
Published 28 November 2025

Abstract

The Laser Interferometer Space Antenna (LISA) will be a space-borne gravitational wave observatory that consists of three spacecraft, separated by several million kilometers, which tracks the separation between inertial test masses via laser interferometry. In this architecture strict requirements exist on the design of the orbits, the ability to accommodate laser frequency noise, the ability to provide the necessary purity of free-fall, and the quality of the optical metrology. This final item is enabled with afocal transmitting/receiving telescopes

* Author to whom any correspondence should be addressed.

that increase the laser power transfer efficiency over the long inter-spacecraft link. These telescopes must be designed and built not to adversely affect the precision of the interferometric measurements. The function, design, and current status of LISA telescopes under development at NASA will be discussed in this article.

Keywords: LISA, gravitational-wave, telescope, interferometry

1. Introduction

Long-baseline laser heterodyne interferometry, on the scale envisioned by Laser Interferometer Space Antenna LISA [1] and other future space-based gravitational-wave observatories, requires the use of telescopes in the observatory arms. Unlike other astronomical telescopes, telescopes of this type are not primarily used to take images of distant objects, but are instead crucial elements of a system geared to performing precise continuous measurements of optical phase changes. These phase changes encode gravitational waves, the sources of which are among the most interesting entities of modern astrophysics.

A key function of the telescopes is to permit sufficient optical power transfer across each inter-spacecraft link, as illustrated in figure 1. Even with the inclusion of large telescopes, there will not be enough light over these distances to directly reflect for a complete round-trip measurement. Instead, it is necessary to operate in a 'transponder' mode, where received light is first detected on the optical bench, a local laser is offset phase-locked to it, and that laser light is used to transmit back towards the distant spacecraft. For reasons of mass and volume efficiency, each telescope operates simultaneously in transmit (Tx) mode and receive (Rx) mode. Each of the three spacecrafts in the LISA constellation hosts two telescopes, making six total flight units: one on each end of each inter-spacecraft arm.

2. Telescopes in the context of LISA

Telescopes in LISA serve to limit the optical losses caused by diffraction of the laser beams over the arm length, by providing a large collecting area for the received beam and a magnified transmitted beam diameter. The optical loss from bench to bench is therefore substantially reduced, and that then allows for the construction of interferometric beat notes of sufficient signal-to-noise to detect optical phase changes due to gravitational waves. However, in performing this key function, the telescopes must not introduce excessive noise to the interferometric measurement system. It is this need for minimal added noise which drives the majority of the design and implementation decisions for the telescopes. These considerations will be explored in greater detail in section 5.

The limiting apertures for each telescope is located on its associated optical bench, such that a telescope acts as a pupil relay, placing the images of those aperture as close as possible to the nominal location of the freely-floating test mass. In effect, the combination of the telescope and the optical bench forms a key optical element in LISA. Interfaces between optical bench and telescope are therefore very important. Such optical interface considerations, as well as mechanical interfaces from each to a common support structure, are described in section 7.

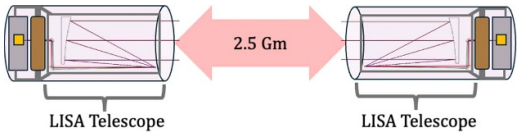

Figure 1. Telescopes enable bi-directional light transfer between optical benches on different spacecraft, across the 2.5 million kilometer separation.

3. Status and future of telescope development

Over the past several years, the LISA telescope has been developed at the NASA Goddard Space Flight Center (GSFC). After several early studies [2–6] and small-scale tests [7–9], an early prototype was created which then served as a pathfinder for studying many important aspects of the telescope [10]. Several interesting preliminary studies were conducted using this prototype, specifically in the areas of optical alignment sensitivities, mirror surface finishes and fabrication, coatings, ground support and test equipment, and scatter. However, despite being an early boon to the LISA telescope development program at NASA, that early prototype unit did not address other important parts of a future LISA telescope, especially as science and engineering requirements matured over the subsequent years.

After the early prototype, a structural thermal model of the telescope (STM) was built as the first unit in a technology development program which was part of the LISA Study Phase at GSFC. In addition to using flight-like materials, it was very nearly the correct size and mass—including appropriate lightweighting. Several tests were performed on the STM telescope, including thermal survival cycling, low-level swept-sine vibrations for modal identification, and early dimensional stability measurements [11, 12]. The STM telescope also served to define the process for creating future LISA telescopes of ever-increasing flight-readiness. These tests ultimately led to an improved understanding of the needs of implementing future flight units.

After the STM telescope, a more realistic version called the engineering development unit (EDU) telescope was created. The EDU telescope (pictured in figure 2) fulfilled many more requirements of the eventual flight units, and including several flight-level optical performance requirements. Much of the work described later in this article pertains to the EDU telescope.

This unit brings us to the current state of the LISA telescope hardware development effort. The next telescope in the path to flight will be an engineering test unit (ETU) which has several advances over the EDU telescope. Firstly, the flight optical design will be used which involves a moderate change from the EDU prescription to allow an on-axis beam exchange between bench and telescope. Another modification between EDU and ETU involves altering the distance between optical bench and telescope, as well as changes in the telescope mechanical bipods to allow mounting into a mechanical structure recently developed by the ESA Prime Contractor. The mechanical interface implemented in the ETU will be ideally being identical to that of future flight mechanical interface. The ETU will undergo a series of rigorous tests aimed at ensuring the unit can meet flight requirements, despite not being scheduled as a primary flight unit. Such an approach is common in spaceflight hardware development and, as such, the ETU will be an early risk-mitigation unit, designed to catch any flaws in the approach or workmanship while there is still time to adjust for the flight units.

The next unit will be a pre-flight unit (PFM) which will also serve as a flight spare. Then the development process moves into flight hardware production. Six flight telescopes, as well as a suitable set of spare parts, will be produced with a high cadence necessitated by flight

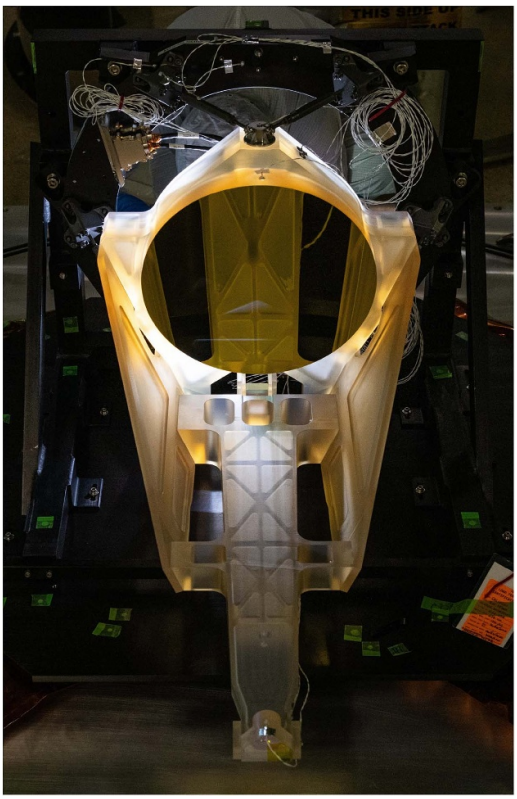

Figure 2. Image of the engineering development unit of the NASA LISA telescopes, delivered in May 2024 to the NASA Goddard Space Flight Center. Image Credit: NASA/Dennis Henry

integration efforts in Europe. These units will be integrated and then will serve for the duration of the mission.

4. Design summary

The telescope can be thought of as a combination of a suitable optical design and an achievable mechanical implementation. Many of the drivers for the telescope design will be discussed in more detail in section 5.

4.1. Optical design

A broad family of observatory needs lead to a set of constraints which inform the design of the LISA telescopes. A suitable optical design is a fundamental part of developing telescopes to meet the needs of LISA. Such an optical design mitigates the coupling of the observatory to undesirable noise sources, while enabling precision long baseline interferometry.

As shown in figure 3, the chosen optical prescription entails an unobstructed off-axis layout which still enables an on-axis beam exchange in either direction. Despite operating as a

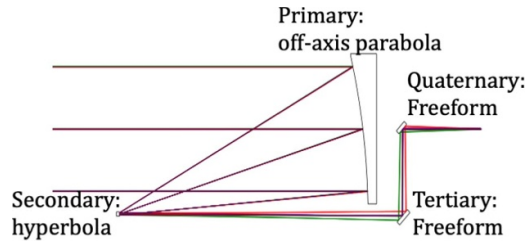

Figure 3. Side view of the future flight telescope prescription. The different ray colors represent the path of light in the different field angles across the acquisition field of view.

transceiver, the telescope mirrors are identified in the traditional sense with the primary being the largest surface and the first encountered in the receiving direction. The primary and secondary mirrors are an off-axis parabola and a hyperbola, respectively. These mirrors share an optical axis, in the classic Cassegrain style. The other two mirrors are freeforms, carefully chosen to reduce the impact of tilt-to-length (TTL) coupling to the LISA long-arm science measurement.

4.2. Mechanical implementation

The optical performance requirements drive the mechanical telescope design. Among the most challenging of these requirements is the need to have extremely high in-band stability (discussed in section 5 in greater detail), while maintaining the ability to align the physical optics as directed by the optical prescription. Several historical studies were conducted, both internally at NASA and with industry partners, which evaluated a multitude of design parameters including, but not limited to, materials, construction techniques, fabricability, and alignment capability. These studies, and the trades they enabled, resulted in a non-standard mechanical design approach where low expansion glass-ceramic was used both as an optical substrate and as a structural material. Very few optical telescopes have been constructed using this approach, with a well-known example being the two-mirror SILEX telescope [13]. In many ways, the LISA flight telescope will be exploring new territory in telescope technology.

After material downselection on the basis of requisite stability, telescope mechanical implementation trades focused on fabricating and assembling the telescope. A monolithic telescope, while attractive from a stability standpoint, could not be implemented with the required optic placement accuracy using current technology. Instead, methods for joining low-expansion brittle parts were investigated. A key guiding principle was that joints should not significantly degrade the in-band stability of the whole structure. A small-scale joint testing program was started to measure this stability, with a noise floor of a few fm $\sqrt{\text{Hz}}^{-1}$ at the relevant frequencies. Various joint approaches and geometries were considered. Ultimately it was decided to use a specialized adhesive joining approach with bond pad thickness oriented perpendicular to the optical path. This approach not only allows for a strong connection between components, but also allows for adjustability of bonding surfaces required for critical mirror alignments during integration.

5. Interferometric noise avoidance as a design consideration

There are a large number of potential noise sources which could be introduced in the interferometric measurement by the telescopes, and which could be mitigated through proper consideration of the telescope design. Understanding and budgeting these noise sources is necessary to ensure that the full system performs as expected.

5.1. Direct optical pathlength noise

Firstly, as shown in figure 1, the telescopes are part of the optical path between benches on different spacecraft. Therefore, optical pathlength variations in the telescopes enter in the same part of the observatory as the gravitational-wave science signal. If those pathlength variations are sufficiently large in the LISA band, they can reduce the signal-to-noise with which the gravitational-wave signals are detected. To counteract this possibility, the stability of the optical pathlength through each telescope is a requirement which flows down from observatory performance budgeting, and is given by:

$$\delta x_{\mathrm{Tel}} \leqslant 1.1\ \mathrm{pm}\,\sqrt{\mathrm{Hz}}^{-1} \times \sqrt{1+\left(\frac{f_0}{f}\right)^4} \tag{1}$$

where $f_0 = 2$ mHz and the frequencies of interest are from $f = 0.1$ mHz to $f = 1$ Hz. Furthermore, this requirement is valid in the presence of all on-orbit driving noise sources, such as temperature noise. The in-band temperature noise, which is one of the major drivers of length instability, is required to be lower than

$$\delta T_{\mathrm{orbit}} \leqslant 5\ \mu\mathrm{K}\,\sqrt{\mathrm{Hz}}^{-1} \times \sqrt{1+\left(\frac{f_{\mathrm{T}}}{f}\right)^4} \tag{2}$$

where $f_{\mathrm{T}} = 2\sqrt{2}$ mHz.

Given that each telescope has roughly 2 m of optical pathlength, a primary clear aperture of approximately 0.3 m, and numerous joints, it is not trivial to achieve and reliably demonstrate this dimensional stability requirement. For example, at frequencies f above f_{T}, achieving optical pathlength noise would require a telescope effective thermal expansion of less than 100 parts per billion per Kelvin. The optical pathlength stability requirement also demands an all-reflecting design, to avoid concerns regarding the coupling of refractive index and temperature noise. This requirement drives several telescope implementation choices, such as the materials selection, and the topology and number of any included joints.

The current solution to is to construct the entirety of the critical metering path out of ultra-low coefficient of thermal expansion material, such as Zerodur glass-ceramic [14], and to keep the number of joints to a minimum, with a four mirror design. This choice of material (which is also used for the LISA optical bench) places a demand upon the platform to keep the telescope close to room temperature. To facilitate this room temperature environment, the primary mirror coating is chosen to be a low-emissivity metallic coating, to minimize the radiative loss of heat to cold space while still providing sufficient optical reflectivity at 1064 nm. The other mirrors are smaller and their coatings are high-reflectivity dielectrics, allowing sufficiently efficient throughput of light transiting the telescope. At delivery, each telescope will have an optical throughput of greater than 87 percent in a ± 1 nm band around the 1064.5 nm laser wavelength, for any linear polarization state. This requirement is only achievable with three laser line dielectric-coated optics, given the necessity of having a gold-coated primary mirror.

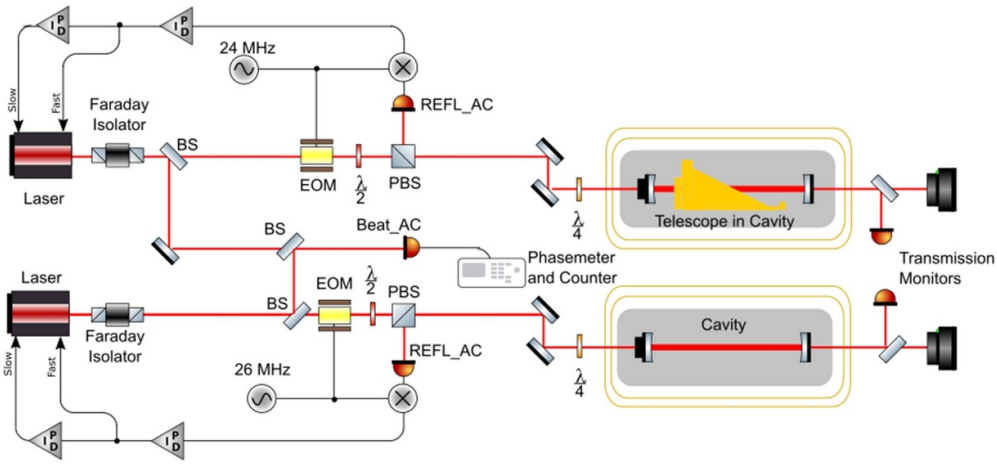

Figure 4. Schematic of the optical pathlength stability test of the telescope units. Optical cavities and control systems are used to convert length changes to frequency jitter, which is then sensed using the heterodyne beat note tracked by a LISA-like phasemeter.

It should be noted that the pathlength noise requirement is levied over any and all causes of optical pathlength change, not just those driven by temperature noise. Many terms are being tracked in a telescope pathlength noise budget, including terms such as coating and substrate Brownian noise, which are not all trivial to calculate given the complicated telescope geometry.

Ultimately, verification of the requirement and the budget roll-up will demand a rather involved test, as well as numerous other early coupon-level concept testing of joints and materials. Similar tests are often performed in other areas of LISA, and the telescope testing will benefit from the expertise and insight gained in those other areas.

To verify this requirement on a real telescope, the telescope will be placed into a large Fabry–Perot cavity. Control loops would then be used to keep a laser resonant with that optical cavity. This method, illustrated in figure 4, converts the telescope optical pathlength noise into frequency noise of the light from that servo-controlled laser. That laser frequency noise can be measured by comparing it to the output of a more stable frequency reference, using an interferometric beat note and a LISA-like phasemeter. Thus, by measuring the relative frequency noise of the two stabilized lasers, the optical pathlength noise of the telescope can be determined. This method has been used on several occasions already—for example, to test smaller design features and joints of the telescope—and has been proven to provide the required sensitivity.

However, in order to show that the telescope will work in the presence of on-orbit temperature noise, it is necessary to go further. Those on-orbit temperature variation limits, of the form presented in equation (2), are difficult to reproduce on the ground. So, a two-pronged approach must be used. Firstly, the in-band temperature noise must be filtered out using a high level of thermal isolation. In that situation, when the optical pathlength noise is measured, the measurement gives the temperature-independent contribution to length noise if other potential sources of measurement imprecision, such as sensing noise, can be made sufficiently small. Then, we separately determine the sensitivity of the optical pathlength to temperature changes by introducing a change in the telescope bath temperature while measuring the corresponding coherent change in the cavity resonant frequency. This measured coupling coefficient between temperature and optical pathlength is used to project the on-orbit temperature noise spectrum to

telescope pathlength noise. Finally, the temperature-independent and temperature-dependent portions of the noise are combined, and compared to the requirement in equation (1).

Filtering out the in-band temperature variations on the ground has been done several times in LISA. Typically, a vacuum chamber is designed to greatly attenuate laboratory temperature perturbations from entering the test. Eliminating convective coupling through appropriately low vacuum levels, conductive coupling through the use of insulating stand-offs, and radiative coupling through the use of nested metal shields, has been proven to provide a sufficiently noise-free temperature environment. For example, a derivation of the thermal transfer function for such a system, used in early investigations of alternative telescope materials, can be found in [8]. A vacuum system with sufficiently low expected in-band temperature noise has been designed and thermally modeled at NASA and will be soon fabricated and commissioned prior to being employed in the testing of telescope dimensional stability.

5.2. Optical backscatter into the science photoreceivers

Another source of interferometric noise is due to scattering of the Tx beam by the telescope optics back into the science interferometer photoreceivers. The local oscillator (LO) on the science photoreceivers is at the same frequency of the Tx beam, having been created from a pickoff of that beam, and this configuration results in an interferometric beat between the Rx and backscattered Tx light which is at the same frequency as the gravitational-wave science beat note between Rx and LO. Jitter in the phase of the backscattered light will produce a small vector noise on the science signal.

To define the scatter limits of the telescope, it is necessary to understand the coupling of telescope scatter to the science signals. The Tx and Rx beams are multiplexed at a polarization beamsplitter (PBS). As illustrated in figure 5, the Tx beam reflets off this PBS towards the telescope, while the Rx beam transmits through the PBS to the rest of the optical bench. The backscatter is expected to be in the same polarization as the Tx beam, and in general reflects at the PBS. Due to finite extinction ratio, and other effects, some portion of the scattered field makes it through the PBS along with the Rx beam.

The science interferometer readout is comprised of a balanced pair of photoreceivers fed from a beamsplitter. Generally, the beam entering this analysis beamsplitter is comprised of a combination of the LO, Rx, and scattered fields. If $\vec{E}_\mathrm{s}$, $\vec{E}_\mathrm{r}$ and $\vec{E}_\mathrm{l}$ are the scattered field, the Rx field, and the LO field respectively at the analysis beamsplitter, the beams from the output ports of the analysis beamsplitter create the signals at each of the two photodiodes given by:

$$S_+ \propto \left| \mathrm{e}^{i\pi} \left[\vec{E}_\mathrm{s} \mathrm{e}^{\mathrm{i}\phi_\mathrm{s}} \mathrm{e}^{\mathrm{i}\omega_\mathrm{s} t} + \vec{E}_\mathrm{r} \mathrm{e}^{\mathrm{i}\phi_\mathrm{r}} \mathrm{e}^{\mathrm{i}\omega_\mathrm{r} t} + \vec{E}_\mathrm{l} \mathrm{e}^{\mathrm{i}\phi_\mathrm{l}} \mathrm{e}^{\mathrm{i}\omega_\mathrm{l} t} \right] \right|^2 \tag{3}$$

$$S_- \propto \left| \left[\vec{E}_\mathrm{s} \mathrm{e}^{\mathrm{i}\phi_\mathrm{s}} \mathrm{e}^{\mathrm{i}\omega_\mathrm{s} t} + \mathrm{e}^{\mathrm{i}\pi} \left(\vec{E}_\mathrm{r} \mathrm{e}^{\mathrm{i}\phi_\mathrm{r}} \mathrm{e}^{\mathrm{i}\omega_\mathrm{r} t} + \vec{E}_\mathrm{l} \mathrm{e}^{\mathrm{i}\phi_\mathrm{l}} \mathrm{e}^{\mathrm{i}\omega_\mathrm{l} t} \right) \right] \right|^2 \tag{4}$$

where a π phase shift between the output ports of the beamsplitter has been explicitly included as a prefactor. Note that the scattered field $\vec{E}_\mathrm{s}$ here is defined at the outputs of the analysis cube, so is much less than the scatter field at the telescope, due to the effect of the PBS multiplexer: $|\vec{E}_\mathrm{s}|^2 = \gamma |\vec{E}_\mathrm{s}^{(\mathrm{Tel})}|^2$, where γ is the suppression ratio of the PBS, typically about 10^{-3}, and the factor of two comes from the analysis beamsplitter. Note also that the LO and Rx beam have the same polarization, while the backscattered beam (which arises from the Tx beam) is in an orthogonal polarization and only makes it to the photoreceivers due to the leakage through the non-ideal PBS. There is a π phase shift for reflecting fields which are in the p-polarization with respect to the analysis beamsplitter, and this brings a relative sign difference between the scattered field and the other two fields.

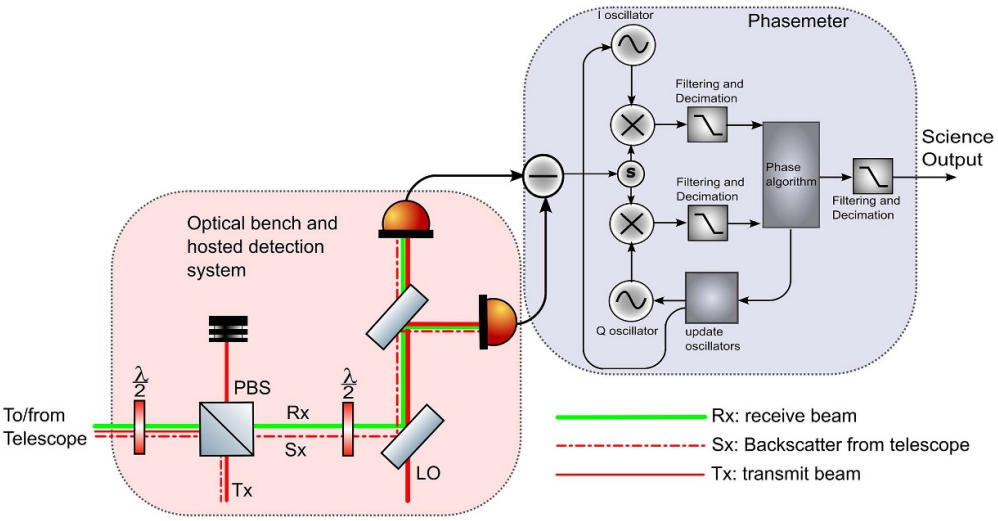

Figure 5. Simplified illustration of the optical detection path in the LISA long-arm measurement. A simplified version of the phasemeter is also shown. A description of the effect of scatter is presented in the text and accompanying equations. The solid red lines are the Tx and LO paths, which are derived from the same beam. The dashed red line is the path of scatter from the telescope. The green line represents the Rx beam path to the photoreceivers.

Expanding equations (3) and (4), and keeping the terms at the heterodyne frequency ω_0, gives:

$$S_{\pm}^{(\omega_0)} \propto \vec{E}_{\rm l}.\vec{E}_{\rm r}\cos\left(\phi_{\rm rl}-\omega_0 t\right) \pm \vec{E}_{\rm s}.\vec{E}_{\rm r}\cos\left(\phi_{\rm rs}-\omega_0 t\right) \tag{5}$$

where the compact notation $\phi_{nk} = \phi_n - \phi_k$ has been used for conciseness. Equation (5) can be re-written as

$$\begin{aligned} S_{\pm}^{(\omega_0)} \propto\ & \vec{E}_{\rm r}.\vec{E}_{\rm l}\left[\cos\left(\phi_{\rm rl}\right)\cos\left(\omega_0 t\right)+\sin\left(\phi_{\rm rl}\right)\sin\left(\omega_0 t\right)\right] \pm \\ & \vec{E}_{\rm s}.\vec{E}_{\rm r}\left[\cos\left(\phi_{\rm rs}\right)\cos\left(\omega_0 t\right)+\sin\left(\phi_{\rm rs}\right)\sin\left(\omega_0 t\right)\right]. \end{aligned} \tag{6}$$

It is immediately evident from equations (5) and (6) that one can construct linear combinations of these signals which are insensitive to the scattered light power, to first order, while remaining sensitive to the gravitational wave science signal. Although addition and subtraction of RF signals is possible, it is prone to many technical issues. As a result, these linear combinations will be performed after demodulation by the RF-tracking phasemeter, whilst treating each signal separately up to that point. Therefore, in this scatter rejection scheme, there are four input channels per science interferometer—the in-phase and quadrature components for each of two detection photoreceivers.

The LISA phasemeter demodulates the sine and cosine components at the heterodyne frequency, and takes the arctangent of the ratio of the demodulated signal. This phasemeter output forms the science signal for that link. To analyze the effect of scattered light on the science signal of this link, we take the ratio of the in-phase and quadrature components which, with the

assumptions of small variations $\{\phi_{\rm rl} \ll 2\pi, \phi_{\rm rs} \ll 2\pi\}$ and small backscatter power relative to the LO power $\left|\vec{E}_{\rm s}\right| \ll \left|\vec{E}_{\rm l}\right|$, becomes

$$\Phi_{\pm} \propto \phi_{\rm rl} \pm \frac{\vec{E}_{\rm s}.\vec{E}_{\rm r}}{\vec{E}_{\rm r}.\vec{E}_{\rm l}}\phi_{\rm rs} \tag{7}$$

The first term in equation (7) contains the gravitational wave signal, while the second is due to the undesirable scatter. Linear combinations of these phasemeter output signals can substantially reduce the scatter term while keeping the science signal intact. In general, such linear combinations will not perfectly eliminate the scatter term, so one is left with:

$$\Phi_{\rm combined} \propto \phi_{\rm rl} + \epsilon_{\rm bal}\frac{\vec{E}_{\rm s}.\vec{E}_{\rm r}}{\vec{E}_{\rm r}.\vec{E}_{\rm l}}\phi_{\rm rs} \tag{8}$$

where $\epsilon_{\rm bal} \ll 1$ represents the degree to which one is able to mitigate the scatter term using linear combinations. Specifically, the second term in equation (8) is the contribution of scatter to the balanced detector. The dot products between the electric fields can be re-written, to extract the effects of both the polarization projection and spatial mode overlap. Also, since the backscattered power depends on the Tx power $P_{\rm Tx}$ entering the telescope, it is convenient to re-cast the scatter contribution in terms of a scatter fraction instead of the scattered power.

$$\Phi_{\rm scatter} = 4\pi\epsilon_{\rm bal}\epsilon_{\rm mode}\sqrt{\frac{\epsilon_{\rm pol}F_s P_{\rm Tx}}{P_l}}\frac{\delta x_{\rm IF}(f)}{\lambda} \tag{9}$$

where the factors $\epsilon_{\rm mode}$ and $\epsilon_{\rm pol}$ are each less than unity, and encode the effects of spatial overlap and polarization respectively. Note that the scatter phase jitter $\phi_{\rm rs}$ has also been re-cast in terms of the interface pathlength variation $\delta x_{\rm IF}$, of the telescope with respect to the optical bench.

As shown in equation (9), the motion $\delta x_{\rm IF}$ of the scatterer is the primary source of the phase noise. This scatter-induced phase noise is governed chiefly by motion of the entire telescope with respect to the plane of the optical bench, as the internal dimension of the telescope is already held to the picometer-scale stability mentioned in equation (1). Motion of the entire telescope, and thus the scatterers, will therefore be dominated by the mechanical interface to the platform. This interface will be further discussed in section 7.

Fundamentally, the equation (9) shows that the effect of scatter on the interferometric signal can be mitigated by:

- highly matched balanced detection
- reducing the displacement noise of the scattering optics (or, more specifically, the pathlength noise experienced by the backscattered light),
- by reducing the overlap of the scattered light with the received field, for a given fixed overlap between received and local fields [15],
- by reducing the fraction of optical power scattered back [2, 6, 15], and the fraction of scatter which goes through the polarizing multiplexer to the photoreceivers,
- and/or by increasing the LO power.

In general, all of these approaches are used in LISA. It is important to note that the phase noise due to backscatter scales linearly with displacement noise, but scales only as the square-root of the scattered power. The key approach is to seek an achievable balance between decreasing the scattered light power and constraining the displacement noise of the interface.

Extensive modeling of scattered power, conservative assumptions on the prefactors $\epsilon_{\rm bal}$, $\epsilon_{\rm pol}$, and $\epsilon_{\rm mode}$, as well as a sub-allocation of interface in-band longitudinal jitter to each of

the telescope and optical bench subsystems, have all combined to produce an allocation for the permissible length noise between the telescope and the rest of the optical system. This pathlength noise allocation is:

$$\delta x_{\mathrm{IF}} \leqslant 30\mathrm{pm}\sqrt{\mathrm{Hz}}^{-1} \times \sqrt{1+\left(\frac{f_0}{f}\right)^4} \tag{10}$$

and is expected to be driven largely by the temperature noise described in equation (2).

The backscattered power $F_s P_{\mathrm{Tx}}$ from the telescope has been extensively modeled using commercially-available non-sequential raytracing software. The scatter is mainly sourced by a combination of particulate contamination on the optical surfaces and by the roughness of the optical surfaces. Of these two scatter sources, particulate contamination—and the resulting Mie scatter—is the dominant contributor to the total backscattered power from the telescope to the optical bench.

The scatter-critical surfaces are the reflective mirrors of the telescope. Physically, surfaces must be both illuminated and viewed by the detector for the scattered power to be important which, for the telescope, is only the case for the optical surfaces. Therefore the cleanliness of these surfaces is very important. The delivery requirement on the optical surface cleanliness levels [16] is CL300 on the primary mirror, and CL200 on the other three mirrors.

Avoidance of scatter is one of several reason to keep the number of telescope mirrors as low as possible, and also a motivation to adopt an unobstructed design.

5.3. Optical pathlength gradient with field angle

Another way that an inadvertent pathlength signal can be created, even in the absence of temperature fluctuations or thermoelastic susceptibility, is due to the laser beam taking a slightly different path through the telescope. This effect is characterized as an optical pathlength gradient with respect to field angle, and can be due to the shapes of the mirrors themselves or to the small lever arm created as pupil shear. This type of effect is one of several forms of TTL coupling—the conversion of angular noise to mean optical phase noise—a topic which will appear several more times in this article.

This gradient of optical pathlength versus field angle is not a typical consideration for a telescope, but in the particular application of LISA, this gradient must be minimized by design. In practice, the gradient itself is effectively static at the measurement frequencies of importance, but at LISA frequencies, in-band field angle variations can interact with the gradient to produce in-band pathlength noise. In Rx, the angular noise input is primarily driven by the angular variation in the spacecraft attitude with respect to inertial space, whereas in Tx, angular noise comes from the interface variations between bench and telescope. These angular noise sources occur on both spacecraft on either end of an inter-spacecraft laser link.

The gradient can be suppressed by careful design of the telescope mirrors, with the inclusion of free-form surface definitions optimized to null this effect [17]. The needed tolerances for the surface-defining polynomial coefficients are well within commercially available capabilities. The overall as-built contribution from this effect to a telescope's TTL coupling is budgeted to be 0.6 mm/rad, including both pupil shear (0.1 mm/rad) and field gradient effects (0.5 mm rad^{-1}), in either angular degree of freedom.

6. Wavefront error (WFE)

Although the telescopes are not implemented for the purposes of capturing images of astrophysical objects, they do still need to provide a very low WFE contribution to the Rx and Tx laser beams. Currently the requirement is to provide a single pass WFE of less than 36 nm RMS, under all possible operating environments. There are four chief considerations which drive the need for a small WFE, two for Tx and two for Rx.

6.1. Telescope WFE considerations

First, one important consideration for Tx WFE is the efficiency of light transfer between spacecraft. The reduction of on-axis intensity due to WFE is given, to a reasonably good approximation [18], by:

$$\frac{I}{I_0} \approx 1 - \frac{4\pi^2 W^2}{\lambda^2} \tag{11}$$

where W is the RMS WFE, $\lambda = 1.064$ μm is the laser wavelength, I_0 is the on-axis intensity in the presence of no wavefront aberrations. Keeping the on-axis power as high as possible, enables a higher ratio of signal to shot-noise in the photodetection at the long arm science interferometer. The combination of a single telescope and a single optical bench provides approximately 53 nm RMS WFE, corresponding to one-twentieth of a wave. This allocation keeps the wavefront-related on-axis intensity loss at less than 10% relative to a hypothetical unaberrated Tx beam.

Second, another wavefront-related consideration is that an aberrated Tx wavefront will produce a phase gradient in the far-field, at the receiving spacecraft. As the transmitting spacecraft's orientation jitters around, due to residual noises in the attitude control system, this phase gradient will sweep across the receiving spacecraft. As the beam has diverged to a diameter of many kilometers across the 2.5 Gm arm, and only the portion illuminating the distant receiving aperture is captured at any given time, this phase gradient very effectively mimics a changing mean optical phase, and therefore could mask gravitational wave signals also encoded in the measured phase. This observatory noise source is a form of TTL coupling, which has been investigated for many years [19], and which can be mitigated by transmitting a beam of sufficiently low aberration content.

Third, even if the wavefront received at the large aperture of the telescope is perfectly flat, the telescope will imprint its WFE in the Rx beam which is provided to the optical bench at the small aperture. In the Rx beam, the presence of WFE can degrade the performance of the long-arm science interferometer. In LISA, this degradation factor is referred to as the 'heterodyne efficiency' η_{het} of the science interferometer, and is calculated as

$$\eta_{\mathrm{het}} = \frac{\iint\limits_S \left(\vec{E}_{\mathrm{r}}^{*} \cdot \vec{E}_{\mathrm{l}}\right) \mathrm{d}A \iint\limits_S \left(\vec{E}_{\mathrm{l}}^{*} \cdot \vec{E}_{\mathrm{r}}\right) \mathrm{d}A}{\iint\limits_S \left|\vec{E}_{\mathrm{r}}\right|^2 \mathrm{d}A \iint\limits_S \left|\vec{E}_{\mathrm{l}}\right|^2 \mathrm{d}A} \tag{12}$$

where the area integration extends over a surface S which limits the interfering beams, for example the spatial extent of the photoreceiver. As evident in equation (12), the amplitude distribution of the individual beams also contributes to degradation of heterodyne efficiency. In practice, as the Rx intensity is essentially uniform after traversing the long arm, while the LO intensity profile is still quite Gaussian, the heterodyne efficiency is not equal to 1, even before the inclusion of aberrations.

Finally, the Rx beam is also used as an orientation reference for the receiving spacecraft, by sampling the interference with the LO on a quadrant photoreceiver and utilizing differential wavefront sensing (DWS). Due to sampling the wavefront over only four quadrants, some wavefront aberrations can be aliased to resemble wavefront tilts, and this can in turn bias the input to the attitude control system. As each spacecraft locally tracks the corresponding far spacecraft by driving this DWS signal to zero, any bias from an aliased WFE will be converted into a pointing error of the TX beam, reducing the amount of power delivered over the link, and also potentially placing the far spacecraft in a steeper portion of the aberration-induced phase gradient mentioned above. Both of these potential consequences increase the noise experienced in that arm.

This last consideration carries importance for the validation of telescope performance in the case of LISA. As the effects of WFE in Rx and Tx are intertwined, they must be simultaneously toleranced in a simulation of the interferometer which forms the inter-spacecraft link. In practice, this is achieved by a Monte-Carlo model of a telescope and associated optical bench, including the environmental sensitivities to perturbations such as temperature changes or gradients, and enforced displacements or rotations of their mechanical interface points. In any given Monte-Carlo instance, all four effects of WFEs, in combination with a host of other tolerances, are evaluated. Then, the performance of the constellation is budgeted against a chosen statistical confidence level. In this way, particularly unfortunate combinations of aberration patterns between the two optical elements will be unlikely to significantly impact the resultant strain sensitivity.

6.2. As-built WFE in the telescope

The WFE of an as-built telescope has three main contributors. Firstly, the optical design has a very small residual error—the design balances several requirements, meaning it is sometimes worthwhile to trade some residual design WFE for better performance in other parameters, such as those related to fabricability and manufacturing—for example, optical placement sensitivities. The second source of WFE is the alignment error of the as-built telescope mirrors into a system. This alignment cannot be done perfectly due to physically-achievable placement resolution of the optics, and so there is some residual WFE. The third source of WFE, and by far the largest for the LISA EDU telescopes, is the surface figure error of the as-built optical surfaces. All mirrors have some surface figure error, usually resulting from the manufacturing process, which results in WFE of the beams transiting the telescope.

In addition to the three main sources of WFE described above, the on-ground testing of the telescopes suffers from an additional source of WFE which is not present in space—the gravity sag of the telescope structure. In a horizontal configuration, the main effects of gravity are a diving-board sag of the boom holding the secondary mirror, and a deformation of the primary mirror due to the tug of gravity on connected structures. To determine the on-orbit telescope WFE map, the gravity sag on ground must be calculated, measured, and removed, as described below.

6.3. Telescope WFE testing

For the specific reasons described in section 6 above, each telescope must produce a sufficiently unaberrated wavefront in both Tx and Rx. When coupled to the difficult internal optical alignment sensitivities of each telescope optic, it becomes clear that measurement of the resulting WFE performance is a necessary step in qualifying each telescope unit for flight. There has been much early work on wavefront measurements from prototype telescopes for LISA in the

past [10]. As the telescope designs have matured, corresponding to solidifying flight requirements, the testing of WFE has become much more detailed. In tandem, these tests have become much more streamlined, rigorous, and sophisticated through the development of ground test software and the use of automation.

The chosen method of measuring the WFE map of each telescope is a double-pass test. A small beam is injected from an interferometer at the small beam side, through the telescope, and retro-reflected off a well-characterized large aperture flat mirror, hereafter referred to as the auto-collimating flat (ACF). The return beam from the ACF goes through the telescope, and is detected at the interferometer. This double-pass method has also been applied to testing previous versions of the LISA telescopes, and is presented in more detail in [10]. The phase front is calculated from four phase-shifted frames using many separate measurements, in a commonplace technique for imaging interferometers. After masking the region of interest using a Boolean filter and fiducials in the data, each phase map is individually unwrapped. The maps are then averaged together, and divided by two to get the single-pass WFE map. At this point, calibration effects such as the WFE signature due to the ACF are subtracted. The process is repeated for several different field angles within the $\pm$ 225 μrad acquisition field of view, with the zero-zero field angle defined to be orientation at which beams at both large and small aperture of the telescopes are parallel to each other.

This double-pass method has been successfully applied to test the EDU telescope which, despite having a slightly different prescription, contains optical surfaces of flight-like quality. The surface figure error contributions of these optical surfaces were carefully budgeted to allow the EDU telescope to successfully meet the flight WFE requirement. As mentioned previously, the residual design WFE for either the EDU or the flight design is small compared to the contribution from surface figure error, so the results of this double-pass test on the EDU are still indicative of the achievable wavefront performance of future units. This type of WFE testing will also be directly applied in the future to the flight telescopes.

In addition to measuring WFE at several different field angles, the EDU telescope was rotated by 180 degrees with respect to gravity and re-tested. This rotation changes the direction of the gravity sag of the telescope, and the sign of the gravity sag aberrations in the WFE maps. The predicted zero-gravity wavefront performance can therefore be accurately determined using appropriate linear combinations of the two sets of WFE maps.

Figures 6 and 7 show the raw WFE maps at a range of field angles within the LISA acquisition field of view, for the original and inverted orientations with respect to gravity. One key takeaway is that the RMS WFE of the telescope does not vary appreciably over the relatively small acquisition field of view. The WFE of the telescope is dominated by the fabrication surface error of the mirrors, rather than the design residual of the optical prescription.

6.4. Comparing different orientations with respect to gravity

Measured wavefront maps in the two orientations are differenced and the result is halved, which directly gives the WFE signature of gravity sag. For example, figure 8 shows the center field measured in each orientation with respect to gravity. Half the difference of the two maps, compared to a prediction from finite element analysis, is shown in figure 9. Note that this differencing method even removes the mid-spatial error, such as polishing striations.

The low order aberration content of the measured gravity signature agrees exceptionally well with the prediction from finite element analysis. The residual error between the predicted and measured errors is largely due to mid-spatial content in the measured maps, which is not part of the finite element analysis.

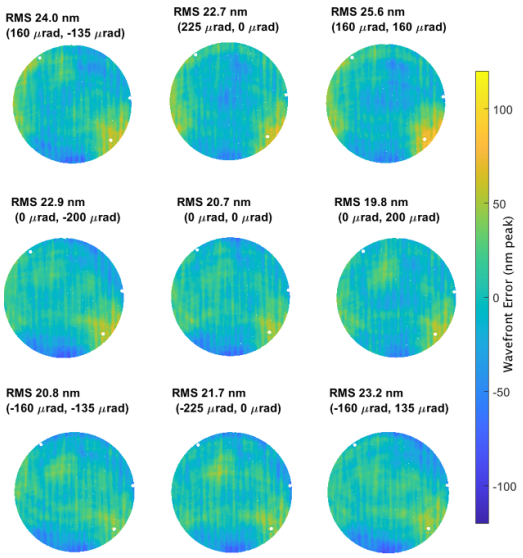

Figure 6. Measured wavefront error maps of the EDU telescope in the original orientation with respect to gravity. The pitch and yaw field coordinates are listed for each map, and range across the acquisition field of view. Each map is 300 mm in diameter.

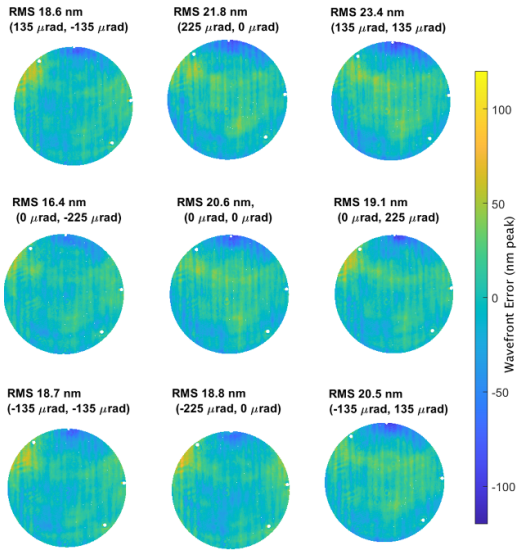

Figure 7. Measured wavefront error maps of the EDU telescope in the inverted orientation with respect to gravity. The pitch and yaw field coordinates are listed for each map, and range across the acquisition field of view. Each map is 300 mm in diameter.

The predicted WFE in a zero-gravity environment can then be determined using the measured WFE maps and the gravity backouts from multi-orientation testing. As an example, the expected zero-gravity WFE at zero field angle is shown in figure 10. The measured RMS error of approximately 20.1 nm is well within the required RMS WFE of 35.5 nm. Furthermore,

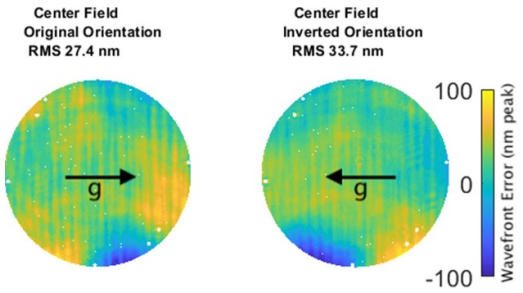

Figure 8. Measured WFE maps of the EDU telescope center field in two opposite orientations with respect to gravity. The maps have been rotated, such that they can be compared and combined appropriately. The black arrows labeled g have been added to indicate the direction of gravity with respect to each map.

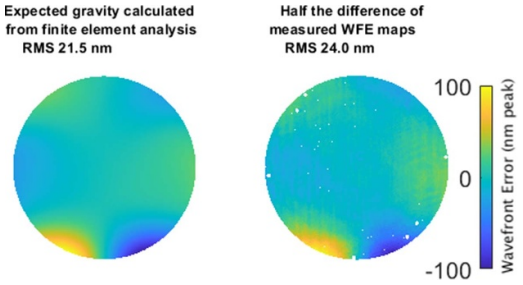

Figure 9. Difference of center-field WFE maps in two orientation with respect to gravity (right), compared to corresponding prediction from finite element analysis (left). The prominent positive and negative peaks at the bottom are largely due to the effect of the M2 tower arm distorting the primary mirror under gravity loading.

these maps have been included into long-arm beam propagation simulations to determine the expected TTL effects, and have been shown to have a sufficiently low aberration content to meet TTL requirements.

7. Opto-mechanical interface considerations

7.1. Optical interface

The science objectives [20] outline the interesting astrophysical sources for observation which, in turn, determine the required strain sensitivity needs of the constellation. This observatory sensitivity includes the acceptable limit due to photon shot noise. And so, once the achievable end-of-life laser power has been determined, the minimum size of the telescope large aperture is essentially fixed. At the same time, there are serious accommodation and technical considerations which constrain the amount of beam expansion that can take place on the optical bench between the fiber injector and the telescope. Once the small beam interface is determined, in combination with the large beam size needs, the telescope magnification becomes fixed. In the current design the small pupil of the telescope is set to a diameter of 2.24 mm, and the large pupil is toleranced to be between 300 mm and 305 mm, resulting in a nominal magnification factor of approximately 135x.

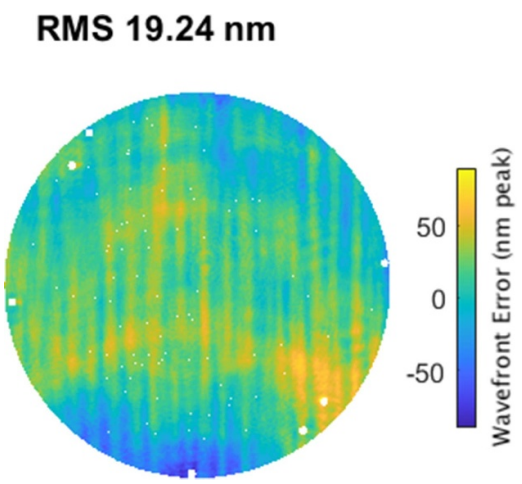

Figure 10. Expected WFE performance of the telescope in a zero-gravity environment for the center field point, formed by taking the mean of the center field maps from the two orientations. The dominant near-vertical striations are due to the fabrication process on the telescope primary mirror. The RMS WFE of this map is 19.24 nm.

The location of these pupils is also a critical interface design issue, as further TTL couplings can be created due to misalignments of the measurement axes between separated optical elements: such as each optical bench and its respective test mass. If a telescope places the pupils improperly, this misalignment could provide a non-negligible TTL coupling. A simple linear coupling exists for the axes transverse to the beam propagation direction, regardless of the location of the rotation point inside the spacecraft, as there will essentially be a lever-arm mismatch between the two interferometers formed on either side of that optical bench. To first order, a misplacement along the axis of propagation does not induce a significant coupling, there is only a residual quadratic term. However, in the presence of an angular bias these longitudinal errors create an effective transverse positioning error, generating a linear term. This angular bias could be due to errors from assembly or environmental perturbations, or in the case of the Tx beam there will at times be a non-zero point-ahead-angle, needed to account for the relative motion of widely-separated spacecraft. These TTL couplings will be driven by angular noise of either the optical sub-assembly with respect to the spacecraft, or of the entire spacecraft with respect to inertia.

Perhaps the easiest way to misplace the large beam laterally is to misplace the entire telescope with respect to the optical bench, for example during payload integration. This is one place where the very high magnification poses a challenge, as every 7.5 μm of error realized here results in a 1 mm offset, and therefore a 1 mm rad^{-1} TTL coupling. For a spacecraft jittering around in orientation at the 10 nrad $\sqrt{\text{Hz}}^{-1}$ level at some frequencies in the LISA band, this already represents 10 pm $\sqrt{\text{Hz}}^{-1}$ of pathlength noise, eclipsing the entire budget for metrology noises and dwarfing the optical pathlength stability expectations for a telescope. In order to bring down the TTL couplings on orbit, from this mechanism or otherwise, the high magnification of the telescope will be leveraged by the inclusion of a Beam Alignment Mechanism (BAM) in each of the Tx and Rx element trains on the optical benches, such that a small adjustment there can introduce a linear TTL coupling which is equal in magnitude but opposite in sign to the sum TTL coupling of that particular as-built payload, compensating as much as

possible the residual length signal in the final data stream. This implementation means that alignment requirements on a telescope are effectively constrained by the range capabilities of this adjustment scheme, rather than final performance targets, with the exception of post-adjustment drifts. As the BAM induced TTL compensation will potentially involve displacing the beams laterally inside the telescope, the mirrors must be oversized to allow for any beam footprint within the anticipated range.

At the small pupil interface, TTL can also couple in due to lateral misalignment, in this case driven by angular instability between the telescope and the optical bench. This leads to a need to have collinear large and small pupils, in line with the beam measuring the distance from the optical bench to the test mass. This is somewhat in conflict with the need to have an unobstructed optical layout to mitigate scattered light impacts, and results in an off-axis prescription which never the less exchanges laser beams in an on-axis geometry.

7.2. Mechanical interface

As with all aspects of LISA hardware, even the mechanical interface is designed with interferometric noise performance in mind. In addition to the aforementioned interface in-band longitudinal noise in equation (10) which was driven by interferometric backscatter mitigation, there is also a TTL-driven in-band interface angular noise requirement. Under the temperature excitation given by equation (2), the angular jitter of the telescope unit in either pitch or yaw must be

$$\delta\psi_{\mathrm{IF}} \leqslant 0.6\mathrm{nrad}\sqrt{\mathrm{Hz}}^{-1} \times \sqrt{1+\left(\frac{f_0}{f}\right)^4} \tag{13}$$

which is not trivial to achieve given the other constraints on the design of the interface. Those other constraints are briefly outlined below.

While the telescope interfaces optically to the optical bench, the mechanical interface is to a common support structure called the MSS, or Movable optical sub-assembly (MOSA) Support Structure. The MSS supports not only the telescope, but also the optical bench, and the gravitational reference sensor, and it has several important and demanding interface requirements. The MSS will be provided by the ESA Prime, and is expected to be discussed elsewhere in greater detail.

The telescopes, like other highly-sensitive space hardware, must be thoughtfully mounted to the MSS. A flexure system is often a suitable choice to fulfill that role, due to the ability to carefully control the interface compliance, thus limiting the forces and motions experienced. Such forces and enforced displacements would otherwise distort the telescope and alter its performance. This flexure approach is the chosen implementation of the telescopes, as is the case with other LISA hardware. The main role of the telescope flexures is to sufficiently isolate the telescope from spacecraft disturbances, both mechanical and thermal in nature, which would otherwise impact telescope performance during science operations, or cause damage during launch.

Mechanical compliance is necessary to avoid transmitting excessive loads into the telescope. However, the allowable compliance is bounded on the high end by the need to decouple the telescopes from spacecraft modes excited during launch. Each telescope, and its mounting structure, must maintain a first vibrational mode of greater than 120 Hz, and this fundamental vibrational mode is largely due to the center of mass motion on the flexures. These two constraints, one in favor of compliance and one limiting compliance, drives the design of a specialized flexure system for the telescope.

Another key design aspect of the telescope mechanical interface is facilitating telescope integration into a MOSA. The alignment requirements are non-trivial. For example, in each of the pitch and yaw degrees of freedom, the telescope to optical bench interface is only permitted to have an error of 65 μrad. Such alignment requirement drive the need for the telescope flexures to be adaptable. During the integration process, the telescope must be positioned with respect to the optical bench using optical metrology techniques, then the telescope flexure system must be attached to the MSS. Therefore, the flexures must be able to be fixed in place, and must not move, when proper alignment between optical bench and telescope is achieved.

Due to stringent magnetic purity requirements on LISA, sourced from the need to avoid electromagnetic forces on the test masses, the telescope mounting structure must also be non-magnetic. Titanium is the chosen material for both the telescope flexure system and the MSS.

One final, and critical, area of consideration for the telescope interface to the MSS is the fact that there is a transition from a brittle glass-ceramic structure of near-zero coefficient of thermal expansion, to a the metallic structure of the MSS. Temperature changes induce thermal expansion and contraction which, at the interface between Zerodur and metal, are not perfectly matched. The flexure design must therefore ensure that any thermal loads due to mismatched thermal expansion imparted into the brittle structures are well-below allowable levels.

The leading design for the telescope mechanical interface realizes all these considerations. While the details of the exact design is proprietary at this time, and cannot be shared in this document, the telescope mechanical interface has been shown to address all these specific needs.

8. Other LISA telescope criteria

There are several other requirements and functional performance objectives of the telescope, some fairly unique. Some are due to aging effects in space, such long term coating loss, while many are related to the environmental disturbances experienced during launch and ascent.

When LISA launches, these telescopes are expected to be the largest all glass-ceramic telescopes ever put into space. Therefore, it is crucial that each telescope is robust enough to survive the forces experienced during launch with no adverse effects and, as a result, a suite of tests will be performed on each flight unit to qualify it for the expected launch environment. This launch environment, and the loads and shocks produced, can be quite demanding on ultrastable brittle structures like the telescopes and optical benches.

Furthermore, even in operation, there will be several perturbations experienced by the telescopes. Variation of the units bulk temperature and temperature gradients, even outside of the science band, will occur. Within bounds, the telescope will be robust to these on-station environmental perturbations.

Unique to LISA, the mass distribution of the telescope must be well-characterized. With freely-floating test masses, the gravitational attraction between the mission's hardware and those test masses must be organized, in a model of the local gravity environment. Each telescope will be scanned, and a point cloud of surface positions will be generated. This information, together with the masses of each sub-component of the telescope, will allow the creation of a telescope mass distribution. Together with similar information from the other hardware in LISA and the LISA MOSA, a gravity balance model can be created. This is yet another example of processes which are not usually considered for traditional telescope developments, but which are necessary for LISA.

An exhaustive list of these types of considerations is beyond the scope of this article, but it is clear that creating LISA's glass-ceramic telescopes is a unique challenge. The boundaries

of traditional telescope development will be expanded, ultimately enabling precision long-baseline gravitational-wave interferometry in space.

9. Conclusion

Telescopes are a crucial part of long baseline laser interferometers in space. In LISA, these telescopes limit the optical losses caused by diffraction of laser beams over the arm length, by providing a large collecting area for the received beam and a magnified transmitted beam diameter. The optical power from bench to bench is therefore substantially increased, and that then allows for the construction of interferometric beat notes of sufficient signal-to-noise to detect optical phase changes due to gravitational waves. However, in performing this key function, the telescopes must not introduce excessive noise to the interferometric measurement system. In fact, it is this need for minimal added noise which drives the majority of the design and implementation decisions for the telescopes.

Data availability statement

The data cannot be made publicly available upon publication because they are not available in a format that is sufficiently accessible or reusable by other researchers. The data that support the findings of this study are available upon reasonable request from the authors.

Acknowledgments

The NASA LISA Telescope team acknowledges substantial beneficial interactions with the LISA Optical Bench team at the United Kingdom Astronomy Technology Centre. The authors also recognize fruitful and collaborative efforts alongside the LISA team at the European Space Agency. The team acknowledges productive discussions with colleagues at the University of Florida. Furthermore, the team acknowledges the substantial expertise in development of the STM and EDU telescopes provided by L3Harris Technologies, Inc. of Rochester, New York. The team also recognizes the important early guidance of Dr Jeffrey Livas (NASA, retired) in the LISA telescope development program. The authors acknowledge that a portion of this work was supported by NASA through the CRESST-II Cooperative Agreement under award number 80GSFC24M0006. Finally, the cohesiveness of the LISA Project Team at NASA GSFC has been vital to the developments described in this work.

ORCID iDs

Kevin Boyce 0000-0002-3980-6066
John Capone 0009-0005-2414-1195
Joseph Howard 0000-0002-2300-6654
Craig Jones 0009-0000-7362-8550
Joshua Lutter 0009-0005-9555-590X
Nova Nimmo 0009-0001-2511-6355
Shannon Sankar 0000-0002-1740-0532

References

[1] Colpi M *et al* 2024 LISA definition study report (arXiv:2402.07571)
[2] Sankar S R and Livas J C 2015 Initial progress with numerical modelling of scattered light in a candidate eLISA telescope *J. Phys.: Conf. Ser.* **610** 012031
[3] Livas J C and Sankar S R 2016 Optical telescope system-level design considerations for a space-based gravitational wave mission *Proc. SPIE* **9904** 538–49
[4] Livas J and Sankar S 2015 Optical telescope design study results *J. Phys.: Conf. Ser.* **610** 012029
[5] Sankar S R and Livas J C 2014 Optical telescope design for a space-based gravitational-wave mission *Proc. SPIE* **9143** 283–9
[6] Livas J, Sankar S, West G, Seals L, Howard J and Fitzsimons E 2017 eLISA telescope in-field pointing and scattered light study *J. Phys.: Conf. Ser.* **840** 012015
[7] Sankar S and Livas J 2016 Testing and characterization of a prototype telescope for the evolved Laser Interferometer Space Antenna (eLISA) *Proc. SPIE* **9904** 99045A
[8] Sanjuan J, Preston A, Korytov D, Spector A, Andreas F, Dixon G, Livas J and Mueller G 2011 Carbon fiber reinforced polymer dimensional stability investigations for use on the laser interferometer space antenna mission telescope *Rev. Sci. Instrum.* **82** 124501
[9] Sanjuán J, Korytov D, Mueller G, Spannagel R, Braxmaier C, Preston A and Livas J 2012 Note: silicon carbide telescope dimensional stability for space-based gravitational wave detectors *Rev. Sci. Instrum.* **83** 116107
[10] Sankar S R and Livas J 2020 Optical alignment and wavefront error demonstration of a prototype lisa telescope *Class. Quantum Grav.* **37** 065005
[11] Umińska A A, Kulkarni S, Sanjuan J, Gleason J, Hollis H, George D, Fulda P and Mueller G 2021 Ground testing of the lisa telescope *Proc. SPIE* **11820** 123–9
[12] Keski-Kuha R A *et al* 2024 Lisa telescope development status and flight design *Proc. SPIE* **13092** 775–83
[13] Juranek H J, Kleer G and Doell W 1994 Use of glass ceramic as a structural material for a high-precision space telescope *Proc. SPIE* **2210** 407–18
[14] Schott ZERODUR product (available at: www.schott.com/en-gb/products/zerodur-p1000269) (Accessed 06 November 2025)
[15] Spector A and Mueller G 2012 Back-reflection from a Cassegrain telescope for space-based interferometric gravitational-wave detectors *Class. Quantum Grav.* **29** 205005
[16] IEST-STD-CC1246 (available at: www.iest.org/Standards-RPs/Recommended-Practices/IEST-STD-CC1246)
[17] Lehan J P, Howard J M, Li H, DeRosa R, Wilson M and Livas J 2020 Pupil aberrations in the LISA transceiver design *Proc. SPIE* **11479** 114790D
[18] Born M and Wolf E 2013 *Principles of Optics: Electromagnetic Theory of Propagation, Interference and Diffraction of Light* (Elsevier)
[19] Bender P L 2005 Wavefront distortion and beam pointing for LISA *Class. Quantum Grav.* **22** S339
[20] LISA Science Study Team 2018 LISA science requirements document *Technical report, Technical Report ESA-L3-EST-SCI-RS-001* European Space Agency